biologia plantarum
an international journal for experimental botany

BIOLOGIA PLANTARUM (2025) 69: 21-37 DOI: 10.32615/bp.2025.003

Physiological, anatomical, and transcriptomic analyses reveal the effects of acid rain stress on *Akebia trifoliata* and the mitigation potential of exogenous curcumin

Xingmei TAO+, Kai WANG+, Xiaoxu BI, and Yongfu ZHANG*

School of Agriculture and Life Sciences, Kunming University, Kunming 650214, China

*Corresponding author: E-mail: 123017360@qq.com

Abstract

This study investigated the impacts of acid rain stress on *Akebia trifoliata* and the mitigation effects of exogenous curcumin (CUR) using integrated physiological, anatomical, and transcriptomic analyses. Acid rain stress significantly decreased chlorophyll content (total chlorophyll by 64.8%), leaf epidermal thickness (upper and lower epidermis by 58.9 and 35.6%), and starch content (by 63.9%), while increasing oxidative stress markers (MDA by 82.6%; ROS production by 345.8%) and content of osmolytes (proline by 64.4%). *A. trifoliata* counteracted acid rain stress by enhancing superoxide dismutase (SOD) and catalase (CAT) activities, and by modifying leaf anatomical structure (increased mesophyll tissue thickness). CUR application, particularly at 50 μmol/L (CUR50), effectively alleviated damage by maintaining leaf structural integrity and promoting growth recovery. Transcriptomic analysis revealed 993 differentially expressed genes between CUR50-treated *vs*. acid rain-stressed plants, primarily enriched in the plant hormone signal transduction and phenylpropanoid biosynthesis pathways. These results demonstrate that CUR mitigates acid rain stress through coordinated physiological adaptations and transcriptional reprogramming of stress-responsive pathways. This study provides a theoretical basis for cultivating *A. trifoliata* and implementing phytoremediation strategies in acid rain-affected regions.

Keywords: *Akebia trifoliata*, curcumin, metabolic pathway, mitigation potential, physiological and biochemical transcriptome.

Introduction

Acid rain is a global ecological issue that has attracted great attention (Xiao et al., 2020). China is the third largest acid rain area in the world after Europe and North America. In China, the area polluted by acid rain has reached 40% of the national land area, with the most prominent region being the south of the Yangtze River and east of Yunnan-Guizhou. This seriously affected agricultural crop growth and biomass production in China (Ren et al., 2021; Yao et al., 2022). Crops exposed to acid rain stress exhibit spot necrosis, anatomical changes, chlorophyll content reduction, and other symptoms of leaf damage (Polishchuk et al., 2016). Moreover, acid rain leads to starch degradation and increased cell membrane permeability. Plants can regulate the content of various osmoregulatory substances

Received 9 January 2025, *last revision* 14 April 2025, *accepted* 2 May 2025.

Abbreviations: 4CL - 4-coumarate-CoA ligase; AHK2_3_4 - *Arabidopsis* histidine kinase 2/3/4; AHP - histidine-containing phosphotransfer protein; ARF - auxin response factor; ARR - two-component response regulator ARR-A family; C3'H - 5-O-(4-coumaroyl)-D-quinate 3'-monooxygenase; CAD - cinnamyl-alcohol dehydrogenase; CAT - catalase; COMT - caffeic acid 3-O-methyltransferase; CUR - curcumin; DEGs - differentially expressed genes; FDR - False Discovery Rate; GH3 - auxin-responsive GH3 gene family; HCT - shikimate O-hydroxycinnamoyltransferase; IAA - auxin-responsive protein IAA; JAZ - jasmonate ZIM domain-containing protein; MDA - malondialdehyde; MYC2 - transcription factor MYC2; PAL - phenylalanine ammonia-lyase; PCA - Principal Component Analysis; POD - peroxidase; SAUR - SAUR family protein; SOD - superoxide dismutase; TCH4 - xyloglucan:xyloglucosyl transferase TCH4; TIR1 - transport inhibitor response 1 protein; TOGT1 - scopoletin glucosyltransferase.

Acknowledgements: The authors would like to thank the National Natural Science Foundation of China (32060645), the Joint Special Project (Key Project) of Local Universities in Yunnan Province (202101BA070000-036), and the Scientific Research Fund of the Ministry of Education of Yunnan Province (2025Y1095). This work was supported by the Kunming University.

+These authors contributed equally.

Conflict of interest: The authors declare that they have no conflict of interest.

including soluble sugars, soluble proteins, and proline to maintain the cellular osmotic balance, thus reducing stress-induced damage to cell membrane (Zhang et al., 2023). Under acid rain stress, absorption of excessive H^+ by plants can easily disrupt the metabolic balance of reactive oxygen species (ROS), leading to rapid accumulation of free radicals and ultimately causing oxidative stress (Ren et al., 2021). To cope with acid rain-induced oxidative stress, plants can regulate the enzymatic antioxidant system including superoxide dismutase (SOD), peroxidase (POD), and catalase (CAT) to scavenge excessive ROS (Kováčik et al., 2011).

Curcumin (CUR), a low-molecular-mass polyphenolic compound isolated from *Zingiberaceae* plants, is widely regarded as a natural antioxidant. It features two phenolic sites that enable immediate scavenging of free radicals, thus mitigating ROS-induced damage (Zaki et al., 2023). CUR plays multifaceted roles in enhancing plant stress resistance, primarily through its antioxidant and antimicrobial properties, which strengthen plants' ability to withstand various environmental stresses and pathogens. It holds significant value for sustainable agriculture (Anas et al., 2024).

Akebia trifoliata is an evergreen woody vine of the *Lardizabalaceae* family, with abundant germplasm resources in Yunnan, Guizhou, and Hunan provinces in China (Zhang, 2024). The whole plant of *A. trifoliata* can be used as medicine. It can be used for detoxification, diuresis, stabilizing the fetus, relieving cough, regulating menstruation, and treating cancer (Jia et al., 2022). It has been planted on a large scale in many parts of China (Cai et al., 2022). It produces high-quality, third-generation fruits rich in amino acids, vitamin C, and other nutrients with sweet taste and unique flavor. This demonstrates that *A. trifoliata*, as both a medicinal plant and an emerging fruit crop, holds significant economic potential.

Currently, studies on *A. trifoliata* mainly focus on the chemical composition, pharmacological activity, nutritional value, resource distribution, DNA fingerprinting, and development of new fruits beneficial for human health (Wu et al., 2018). The tolerance of *A. trifoliata* to acid rain stress and its response to exogenous addition of CUR are unclear. The lack of molecular biology studies and relative scarcity of genetic information of *A. trifoliata* have severely limited its subsequent development and utilization. Therefore, we hypothesize that exogenous application of CUR may alleviate the detrimental effects associated with acid rain stress on plants. *A. trifoliata* cuttings were used for pot experiments, and acid rain stress was simulated after watering CUR on *A. trifoliata* roots. Alterations in the morphology, anatomical structure, contents of photosynthetic pigments and osmoregulatory substances, and activity of antioxidant enzymes were assessed. Transcriptome sequencing analysis was performed using the *Illumina Novaseq 6000* platform, and bioinformatics analysis of the sequencing results was conducted using public databases to explore the mechanisms underlying *A. trifoliata*'s response to acid rain stress and the role of exogenous CUR. This study aims to provide a theoretical basis for the widespread cultivation of *A. trifoliata* and phytoremediation in acid rain-prone regions.

Materials and methods

Plants and treatments: *A. trifoliata* cuttings used in this experiment were obtained from the germplasm resource nursery of *Dongfang Farm Management Bureau* in Mile City, Yunnan Province. CUR was purchased from *Shanghai Macklin Biochemical Technology Co.* Five treatments were set up: the control group (Control) received neither CUR treatment nor acid rain stress, the CUR0 group was exposed to acid rain stress alone, while the CUR25, CUR50, and CUR100 groups were treated with CUR at concentrations of 25, 50, and 100 μmol/L, respectively, under acid rain stress conditions. Each treatment included four healthy plants with consistent growth and height of approximately 110 cm. They were planted in individual white pots (length 100 cm, width 30 cm, and depth 25 cm). According to the main rainfall components of acid rain in Southwest China, sulfuric acid and nitric acid (in the molar ratio of $SO4^{2-}$:NO_3^- = 5:1) were used to simulate acid rain (Zhou et al., 2017). A pre-test was conducted before the formal experiment. The pH of the simulated acid rain was set at 2.0. At 7:00 h, *A. trifoliata* roots were first watered with different concentrations of CUR solution (500 mL) or an equal amount of distilled water for Control and CUR0. Watering was repeated every 2 days. At 18:00 h on the same day of watering, the plants were sprayed with simulated acid rain until all leaves had liquid droplets. Control was sprayed with an equal amount of distilled water, and the treatment was stopped after 28 d. For further analysis, the 10^{th} - 15^{th} leaves counted upward from the bottom of the plant were collected at 6:00 h 3 d later. After collection, leaf segments of 0.6 cm^2 area in the middle were cut along both sides of the main veins and quickly fixed in FAA (90 mL of 70% ethanol + 5 mL of formaldehyde + 5 mL of glacial acetic acid) to maintain the original state of the samples for anatomical structural observation. The other parts were immediately used to measure the activities of SOD, POD, and CAT. The remaining samples were wrapped in tinfoil, snap-frozen in liquid nitrogen, and stored at -80°C for the determination of remaining physiological indexes and transcriptome sequencing.

Measurement of growth indicators: The plant height was measured using a tape measure. The stem diameter was measured using a vernier caliper at 2 cm above the ground. The plant was pulled out from the substrate, washed with water, and dried at room temperature. The root was separated from aboveground part using scissors. Fresh masses of the aboveground part and root were determined, and the root length was measured using a tape measure. The whole aboveground part was dried in an oven at 105°C for 0.5 h and further dried at 85°C until constant mass, which was noted as the dry mass.

Measurement of chlorophyll content: *A. trifoliata* leaves (0.1 g) were cut and placed in 5 mL of 95% ethanol.

The extraction was performed in dark until the leaves whitened. The absorbance of the extract was measured at 665 and 649 nm to calculate the contents of chlorophyll *a* and chlorophyll *b*, respectively (Zou, 2000).

Measurement of malondialdehyde (MDA) content and production rate of oxygen free radicals: Leaf sample (1 g) was ground with trichloroacetic acid and centrifuged. To 2 mL of supernatant, thiobarbituric acid solution was added, placed in boiling water bath, cooled, and centrifuged at 4 000 × *g*. The absorbance of the supernatant was measured at 532, 600, and 450 nm. The MDA content was calculated using the method described by Kumar and Knowles (1993).

Leaf sample (1 g) was ground with potassium phosphate buffer and centrifuged at 10 000 × *g*. To 0.5 mL of supernatant, hydroxylamine hydrochloride was added and incubated in a water bath. Further, sulfonamide and α-naphthylamine were added for color reaction. After centrifugation, the absorbance was measured at 530 nm. The production rate of oxygen free radicals was calculated according to the method described by Zhang et al. (2009).

Measurement of physiological indexes related to stress tolerance: SOD activity was determined using the nitroblue tetrazolium (NBT) method (Li, 2000). We transferred 0.2 mL of the enzyme solution to a centrifuge tube, and sequentially added phosphate-buffered saline (PBS), methionine (MET), NBT, EDTA-Na_2, riboflavin, and distilled water. For the control tube, the enzyme solution was omitted. We incubated the tubes at 25 - 35°C under light exposure for 20 - 30 min. After the reaction, we measured the absorbance at 560 nm using a microplate reader.

POD activity was measured using the guaiacol method (Li, 2000). PBS was mixed with guaiacol and heated until it was dissolved. After cooling, 30% hydrogen peroxide (H_2O_2) was added. 20 µL of the enzyme solution was combined with 1 mL of the reaction mixture, and the absorbance was measured at 470 nm. Data were recorded every 30 s.

CAT activity was determined by the ultraviolet absorption method (Zou, 2000). 0.1 g of leaves was homogenized and enzyme solution was extracted with 10 mL of PBS (0.05 mmol/L, pH 7.8). The mixture was centrifuged at 4 000 × *g*, and the supernatant was collected. The reaction system consisted of PBS (0.15 mmol/L, pH 7.2) and 30% H_2O_2. 20 µL of the enzyme solution was added to 200 µL of the reaction mixture, and the absorbance was measured at 240 nm. Data were recorded every 30 s.

Soluble sugar content was quantified using the anthrone colorimetry method (Gao, 2006). To 0.1 g of dried leaf powder distilled water was added, and then boiled in a water bath for 20 min. After cooling, the solution was filtered into a 100-mL volumetric flask and diluted to the mark. 0.2 mL of the sample solution was transferred to a test tube, 2.3 mL of distilled water was added, and mixed thoroughly. 6.5 mL of anthrone reagent was added, shaken to develop color, and the absorbance was measured at 620 nm.

Starch content was determined by the perchloric acid hydrolysis method (Du et al., 2020). The residue from soluble sugar extraction was transferred to a 50-mL volumetric flask. 20 mL of distilled water was added, and sample was boiled for 15 min. 2 mL of 9.2 mol/L perchloric acid was added and the extraction continued for 15 min. After cooling and centrifugation, the supernatant was collected. The supernatant was mixed with 6.5 mL of anthrone reagent to develop color, and the absorbance was measured at 620 nm.

Soluble protein content was measured using the *Coomassie Brilliant Blue G-250* staining method (Gao, 2006). Leaves (0.1 g) were homogenized and extracted with 10 mL of PBS (0.05 mmol/L, pH 7.8). The mixture was centrifuged at 4 000 × *g* and the supernatant was collected as the crude protein extract. After adding 200 µL of *Coomassie Brilliant Blue* solution to 40 µL of the extract, the absorbance was measured at 595 nm.

Proline content was determined using the acidic ninhydrin method (Wang, 2024). Leaves (0.1 g), were cut into small pieces and placed in a centrifuge tube. 5 mL of 70% ethanol was added and incubated in a water bath for 15 min. After cooling and centrifugation at 4 000 × *g*, the supernatant was collected and mixed with 0.2 mL of acidic ninhydrin and 0.2 mL of glacial acetic acid. The mixture was boiled for 15 min, cooled and extracted with 4 mL of toluene. The absorbance of the proline-toluene solution was measured at 515 nm.

Measurement of anatomical parameters of leaves: The fixed leaf samples were dehydrated, turned transparent, soaked in wax, embedded, and further sliced using a *KD-2258* rotary slicer (thickness = 8 µm). The slices were glued, baked, dewaxed, stained with saffron-green, sealed with neutral gum, and observed using an *Olympus CX41* optical microscope. *Image J* was used for data measurement and image acquisition. The thickness of upper epidermis, lower epidermis, leaves, palisade tissue, and spongy tissue was measured. The mean value of each parameter from each slice was considered to represent the final measurement value, and the ratio of palisade/spongy tissue was calculated according to Hu et al. (2022).

Transcriptome sequencing and bioinformatic analysis:

Total RNA extraction, library establishment, and sequencing: The total RNA was extracted from 1 g of *A. trifoliata* leaves using the *MJZol* total RNA extraction kit (*Shanghai Major Biomedical Technology Co.*, China). RNA integrity and DNA/protein contamination were analyzed using agarose gel electrophoresis. RNA purity (A_{260}/A_{280} and A_{260}/A_{230} ratios) was measured using an ultra-micro spectrophotometer, and the RNA Integrity Number (RIN) was evaluated using the *Agilent 5300 Series Bioanalyzer*. After passing the test, the library establishment and non-parametric transcriptome sequencing were commissioned to *Shanghai Major Biomedical Technology Co*.

Data quality control and de novo assembly: The cDNA library of *A. trifoliata* leaf tissue was subjected to high-

throughput sequencing analysis using *Illumina Novaseq 6000* sequencing platform. The raw reads obtained from sequencing were subjected to quality control, which was done by removing low-quality reads, junction contamination, reads with high number of unknown base N, low-quality reads, and reads with all A bases. Therefore, high-quality clean reads were obtained that could be used for subsequent analyses. *De novo* assembly of the clean reads was performed using *Trinity*. The assembled transcripts were clustered and subjected to de-redundancy using *Tgicl* to obtain the unigenes, which were used as the reference sequences for subsequent analyses (Qian et al., 2022). Additionally, the assembly quality of all unigenes was evaluated, including GC content, Q20, and Q30.

***Analysis of gene expression**:* The assembled reference sequences were mapped back to the transcriptome using *Bowtie2* (Langmead and Salzberg, 2012). The RNA-seq data from *A. trifoliata* leaf tissues were aligned and quantified using the *RSEM* software, and the normalized expression levels of genes and transcripts were calculated using the TPM (transcripts per million) formula (Li and Dewey, 2011). Further, the differential expression analysis was conducted using *DESeq2*. The DEGs (differentially expressed genes) were screened as per the criteria of FDR (false discovery rate) < 0.05 and gene expression fold change $|\log_2 FC| \geq 1$ to compare the differences between different treatment groups. *KEGG* pathway enrichment analysis was performed using the DEGs. Metabolic pathways with corrected $P_{adjust} < 0.05$ were considered significant pathways.

The raw transcriptome data have been uploaded to the *GEO* database of *NCBI* (https://www.ncbi.nlm.nih.gov/geo/info/submission.html), and the *GEO* accession number is GSE294141.

Data processing and analysis: All experimental data were recorded and organized using *Microsoft Excel 2019* and further statistically analyzed using *SPSS 27.0*. The results were expressed as mean ± standard deviation (SD). One-way *ANOVA* and *Duncan*'s multiple comparisons were used to analyze the significance of differences in various indicators between different treatments. $P<0.05$ was considered significant. The principal component analysis (PCA) of physiological indexes was performed by dimensionality reduction method. Plots were drawn using *Origin 2021* and *Graphpad Prism9*.

Results and analysis

Morphological characteristics of *A. trifoliata* under acid rain stress and CUR treatment: The morphological characteristics of *A. trifoliata* under acid rain stress and CUR treatment were observed on the 28th d of treatment. Compared with Control, the plants in CUR0 exhibited a large number of white-brown spots, chlorosis, yellowing of leaves, plant wilting, severe reduction in the number of fibrous roots, and slow root development. Under CUR treatment, the symptoms related to acid rain stress were alleviated to various degrees (Fig. 1*A*,*B*). Compared with CUR0, CUR25 and CUR50 treatments significantly reduced the necrotic spots of *A. trifoliata*, and the root morphology was closer to that of Control. Compared with CUR0, the plant height, stem diameter, fresh and dry weights of aboveground parts, and root length and root fresh weight of plants in CUR25 and CUR50 increased by 26.48% and 33.45% ($P<0.05$, Fig. 1*C*), 47.40% and 50.65% ($P<0.05$, Fig. 1*D*), 25.50% and 28.90% ($P<0.05$, Fig. 1*E*), 41.92% and 58.46% ($P<0.05$, Fig. 1*F*), 72.30% and 63.45% ($P<0.05$, Fig. 1*G*), and 191.09% and 228.80% ($P<0.05$, Fig. 1*H*), respectively. However, in plants in CUR100, the restoration of symptoms related to acid rain stress was significantly reduced, and leaf spot necrosis was significantly increased compared to CUR25 and CUR50. Moreover, the root system was severely distorted (Fig. 1*B*).

Physiological and biochemical indexes of *A. trifoliata* leaves under acid rain stress and CUR treatment: Compared with Control, the content of chlorophyll *a*, chlorophyll *b*, total chlorophyll, and starch decreased by 58.16, 77.88, 64.77, and 63.85%, respectively, and content of soluble sugar, soluble protein, proline, and MDA, production rate of oxygen free radicals, and activities of SOD and CAT increased by 43.20, 44.55, 64.40, 82.55, 345.77, 44.20, and 34.78%, respectively ($P<0.05$, Fig. 2*D-F*), in the leaves in CUR0.

Compared with CUR0, the content of chlorophyll *a*, chlorophyll *b*, and total chlorophyll and activities of SOD, POD, and CAT increased by 51.02, 154.75, 72.84, 93.69, 145.61, and 93.25%, respectively; the content of soluble sugar, soluble protein, proline, and starch increased by 30.19, 55.36, 88.98, and 57.36%, and MDA and production rate of oxygen free radicals decreased by 18.13 and 54.18%, respectively ($P<0.05$, Fig. 2) in CUR25.

Compared with CUR0, the content of chlorophyll *a*, chlorophyll *b*, total chlorophyll, soluble sugar, soluble protein, proline, and starch and activities of SOD, POD, and CAT increased by 71.03, 175.31, 92.97, 93.33, 108.62, 198.39, 142.55, 130.74, 276.22, and 155.02%, respectively ($P<0.05$, Fig. 2*D-G*); MDA content and production rate of oxygen free radicals decreased by 40.68 and 60.14%, respectively ($P<0.05$, Fig. 2) in CUR50.

However, the content of chlorophyll *a*, total chlorophyll, soluble sugar, soluble protein, proline, and MDA were not significantly different in the leaves in CUR100 and CUR0 ($P>0.05$, Fig. 2*A*,*C-F*,*H*). The contents of chlorophyll *b* and starch were significantly lower and production rate of oxygen free radicals was significantly higher in CUR100 than in CUR25 and CUR50 ($P<0.05$, Fig. 2*B*,*G*,*I*). SOD activity was 24.04 and 36.24% lower and POD activity was 47.22 and 65.54% lower in CUR100 than in CUR25 and CUR50, respectively ($P<0.05$, Fig. 2*J*,*K*).

Overall, acid rain stress accelerated degradation of chlorophyll and starch and caused severe osmotic and oxidative stresses. Under acid rain stress, increased content of soluble sugar, soluble protein, proline, and other

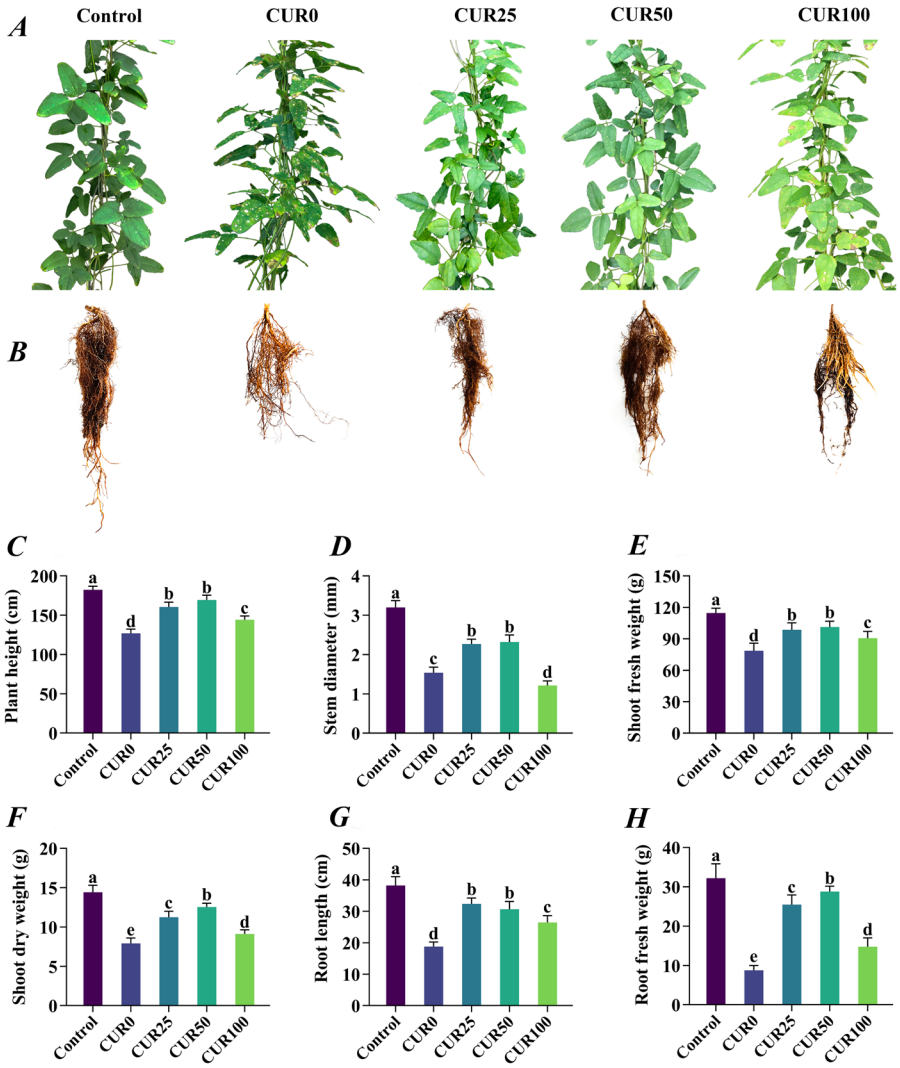

Fig. 1. Morphological features of *A. trifoliata* plants treated with different concentrations of CUR. *A*: morphology of aboveground part; *B*: morphology of root system; *C-H*: alterations in morphological indicators. One-way *ANOVA* was performed to compare the significant changes between treatments, and the results are displayed as means ± SDs ($n = 4$). Control group is Control; CUR0: treated with simulated acid rain having a pH of 2.0; CUR25: treated with simulated acid rain of pH 2.0 and 25 μmol/L curcumin; CUR50: treated with simulated acid rain of pH 2.0 and 50 μmol/L curcumin; CUR100: treated with simulated acid rain of pH 2.0 and 100 μmol/L curcumin. There are significant variations between the lowercase letters in the bar chart at the $P<0.05$ level.

osmoregulatory substances and activities of antioxidant enzymes (*e.g.*, SOD, POD, and CAT) were more conducive to coping with acid rain stress. CUR could effectively slow down the chlorophyll degradation rate, increase content of osmoregulatory substances and antioxidant enzyme activities to maintain the osmotic balance and reduce the degree of cell membrane lipid peroxidation, and alleviate the damage to *A. trifoliata* due to acid rain stress.

Comprehensive evaluation of the physiological indexes using principal component analysis: To analyze the differences and correlations between physiological indexes and different concentrations of CUR, PCA was performed. PC1 and PC2 explained 51.00 and 44.30% of the total variance, respectively (Fig. 3). No significant difference was observed between CUR100 and CUR0 as well as between CUR25 and CUR50 ($P>0.05$, Fig. 3). However, some of the physiological indexes of CUR25 and CUR100 were not significantly different from each other ($P>0.05$, Fig. 3), whereas CUR50 and CUR100 were significantly separated from each other ($P<0.05$, Fig. 3). Additionally, the Control group was significantly separated from the CUR groups ($P<0.05$, Fig. 3). PCA indicated significant positive correlation between activities of SOD, POD, and CAT and soluble sugar content. A significant positive correlation was observed among the content of starch, chlorophyll *a*, chlorophyll *b*, and total chlorophyll content. Production rate of oxygen free radicals and MDA content were significantly positively correlated ($P<0.05$, Fig. 3). The results revealed that the effect of CUR50 was the most significant.

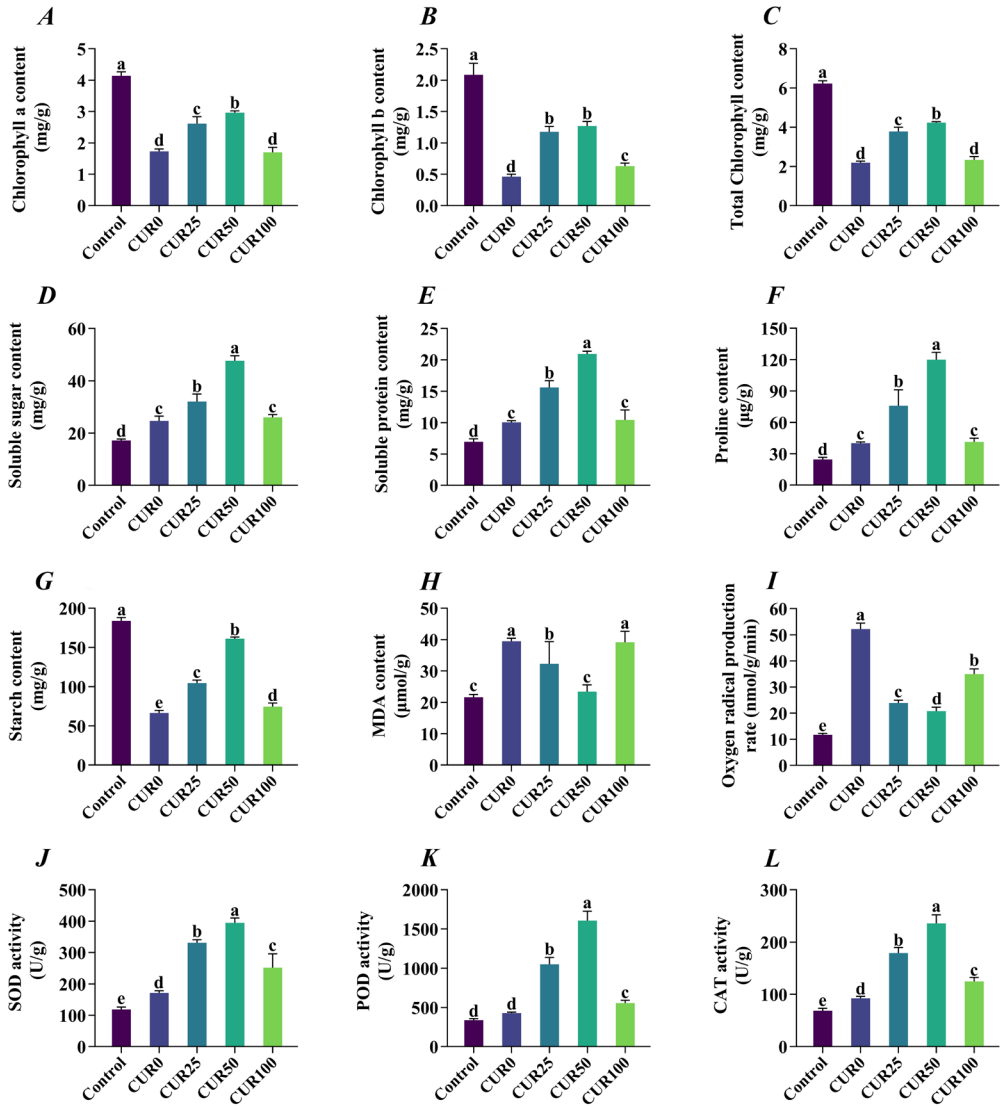

Fig. 2. Physiological indicators of leaves of *A. trifoliata* treated with different concentrations of CUR. *A-C*: chlorophyll content; *D-G*: content of osmotic adjustment substances; *H-I*: content of membrane lipid peroxides; *J-L*: activity of antioxidant enzymes. One-way *ANOVA* was performed to compare the significant changes between treatments, and the results are displayed as means±SDs (n=4). Control group is Control; CUR0: treated with simulated acid rain having a pH of 2.0; CUR25: treated with simulated acid rain of pH 2.0 and 25 μmol/L curcumin; CUR50: treated with simulated acid rain of pH 2.0 and 50 μmol/L curcumin; CUR100: treated with simulated acid rain of pH 2.0 and 100 μmol/L curcumin. There are significant variations between the lowercase letters in the bar chart at the P<0.05 level.

Anatomical structural changes in *A. trifoliata* leaves under acid rain stress and CUR treatment: To more comprehensively analyze the changes in *A. trifoliata* leaves under acid rain stress and the mitigation effect of CUR, anatomical structural changes were observed in *A. trifoliata* leaves in Control, CUR0, and CUR50. In the leaves in Control, the epidermis consisted of one layer of tightly arranged, regular shaped flat cells without intercellular spaces, and a distinction was observed between upper and lower epidermis (Fig. 4*B*). The mesophyll consisted of palisade and spongy tissues. The leaf was a typical bifacial leaf, with lateral veins. Palisade tissues consisted of 1 - 2 layers of long columnar or ellipsoid cells, which were tightly arranged and perpendicular to the cells of the upper epidermis. Spongy tissue was located under the palisade tissues, immediately adjacent to the lower epidermis; the cells were irregularly shaped, connected with each other to form a mesh, loosely arranged, and similar to sponges in appearance.

Interestingly, the leaf structures of Control, CUR0, and CUR50 significantly differed. Compared with Control, the lateral veins and epidermis of leaves in CUR0 were severely damaged and structurally incomplete; most of the palisade tissues were composed of two layers of long columnar cells arranged tightly, with tightly packed cells and small intercellular spaces (Fig. 4*D*). In CUR50, the degree of damage to the epidermis and lateral veins of leaves was significantly reduced; however, the palisade

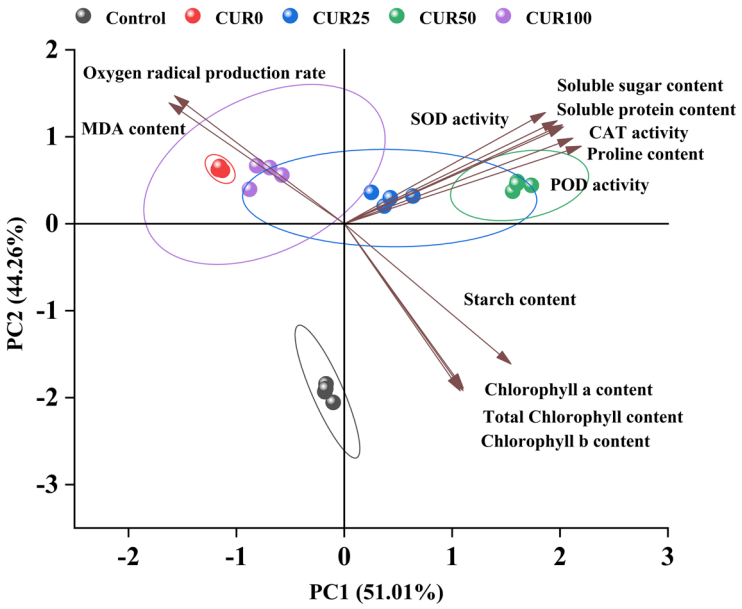

Fig. 3. Results of principal component (PCA) comprehensive evaluation of physiological indexes of leaves of *A. trifoliata* treated with different concentrations of CUR. The confidence circle in the figure is at the 0.95 level. Control group is Control; CUR0: treated with simulated acid rain having a pH of 2.0; CUR25: treated with simulated acid rain of pH 2.0 and 25 μmol/L curcumin; CUR50: treated with simulated acid rain of pH 2.0 and 50 μmol/L curcumin; CUR100: treated with simulated acid rain of pH 2.0 and 100 μmol/L curcumin.

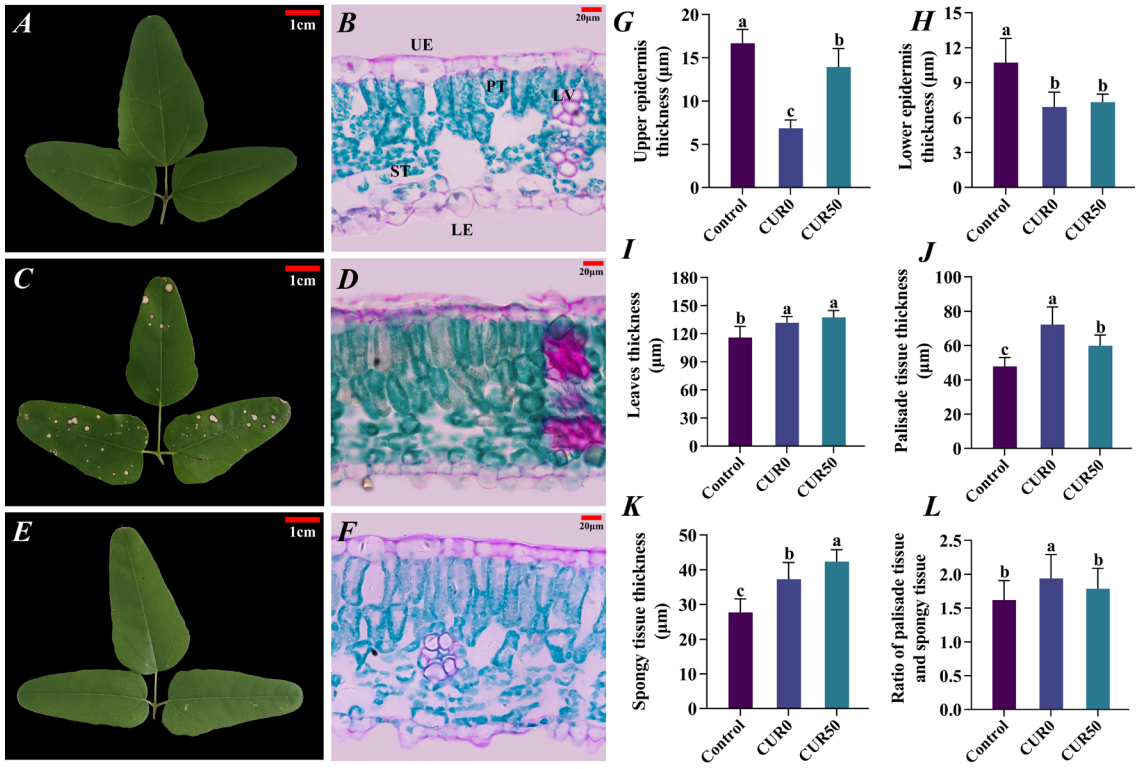

Fig. 4. Leaf morphology and mesophyll anatomical structure of *A. trifoliata* leaves treated with different concentrations of CUR. *A* and *B* served as control groups, while *C* and *D* were treated with simulated acid rain at pH 2.0. Groups *E* and *F* received combined treatment with pH 2.0 simulated acid rain and 50 μmol/L curcumin. *A*, *C*, and *E*: leaf morphology; *B*, *D*, and *F*: leaf mesophyll tissue; *G-L*: leaf mesophyll anatomical structure indexes. UE: upper epidermis; LE: lower epidermis; PT: palisade tissue; ST: spongy tissue; LV: lateral veins. The scale bar for leaves is 1 cm, and for anatomical structures, it is 20 μm. The staining agents used were safranin and fast green. Control group is Control; CUR0: treated with simulated acid rain having a pH of 2.0; CUR50: treated with simulated acid rain of pH 2.0 and 50 μmol/L curcumin.

tissues were basically composed of two layers of columnar cells in a compact arrangement (Fig. 4*F*).

Quantitative analysis was performed on leaf epidermis and mesophyll cells. Compared with Control, the thickness of the upper and lower epidermis in CUR0 decreased by 58.93 and 35.57%, respectively; thickness of leaf, palisade tissue, and spongy tissue and the ratio of palisade/spongy tissue increased by 13.75, 50.75, 34.58, and 19.90%, respectively ($P<0.05$, Fig. 4*G-L*). Compared with CUR0, the thickness of upper epidermis and spongy tissue in CUR50 increased by 103.66 and 13.50%, respectively ($P<0.05$, Fig. 4*G*,*K*); however, the lower epidermis and leaves thickness was not significantly different ($P>0.05$, Fig. 4*H*,*I*), and palisade tissues thickness and ratio of palisade/spongy tissues decreased by 17.02 and 7.84%, respectively ($P<0.05$, Fig. 4*J*,*L*). No significant difference was observed in the ratio of palisade/spongy tissues between CUR50 and Control ($P>0.05$, Fig. 4*L*).

In conclusion, the decrease in the thickness of the leaf epidermis of *A. trifoliata* is a manifestation of its suffering from acid rain stress. However, an appropriate concentration of CUR can effectively mitigate the damage to the leaf epidermis and lateral veins of *A. trifoliata* caused by acid rain stress.

Transcriptome sequencing of CUR-treated *A. trifoliata* leaves:

Assessment of transcriptome sequencing data: To investigate the mechanism by which *A. trifoliata* responded to acid rain stress and CUR enhanced its stress resistance at the gene level, non-parametric transcriptome sequencing was performed on *A. trifoliata* leaves of Control, CUR0, and CUR50 with three biological replicates. A total of nine cDNA libraries were constructed, with a total of 63.10 Gb of clean data and more than 6.52 Gb of clean data per sample (Table 1). For the Control group (Control_1, Control_2, and Control_3), 47 644 476, 44 619 286, and 49 530 660 high-quality clean reads were obtained, respectively. For the CUR0 (CUR0_1, CUR0_2, and CUR0_3) and CUR50 (CUR50_1, CUR50_2, and CUR50_3) groups, 48 197 900, 49 175 852, 45 072 782, 49 848 580, 45 473 614, and 43 646 352 high-quality clean reads were obtained, respectively (Table 1). The average error rate of sequencing bases corresponding to clean data was less than 0.05%; the Q20 and Q30 of each sample exceeded 97.00 and 93.00%, respectively, and the GC content of total bases of clean data in each sample reached >44.00% (Table 1). These results indicated that the high-throughput sequencing platform for transcriptome sequencing of *A. trifoliata* could provide high quality and quantity of data, which could be used for the subsequent *de novo* assembly and transcript quantification.

The *Trinity* software was used for sequence assembly of sample data. In total, 127 383 transcripts were obtained, with an average length of 1 087.77 bp and N50 length of 1 826 bp (Table 1 Suppl.). The obtained transcripts were further assembled to obtain 82 321 unigenes, with an average length of 925.22 bp and N50 length of 1 623 bp (Table 1 Suppl.). The filtered clean reads of each sample were compared with the reference sequences obtained from *Trinity* assembly, and the number of clean reads that could be matched to the assembled transcripts ranged from 17 294 801 to 19 765 848 with the matching efficiency ranging from 79.16% to 80.00% (Table 2 Suppl.). Overall, the transcriptome sequencing and assembly integrity were sufficiently good for subsequent analysis.

Gene expression analysis: Differential expression analysis using *DESeq2* identified differentially expressed genes (DEGs) among Control, CUR0, and CUR50 (with thresholds of $|\text{Log2FC}| \geq 1$ and FDR < 0.05), as shown in Fig. 5*A-D*. The results showed 2 978 DEGs in the CUR0 *vs.* Control comparison, including 1 561 upregulated and 1 417 downregulated DEGs; 3 145 DEGs in the CUR50 *vs.* Control comparison, with 1 719 upregulated and 1 426 downregulated DEGs; and 993 DEGs in the CUR50 *vs.* CUR0 comparison, including 536 upregulated and 457 downregulated DEGs. We observed 1 523 shared DEGs between the CUR0 *vs.* Control and CUR50 *vs.* Control comparisons, 489 shared DEGs between the CUR50 *vs.* Control and CUR50 *vs.* CUR0 comparisons, and 312

Table 1. Statistics of transcriptome sequencing data of *A. trifoliata* leaves. Following the clean reads, which are high-quality sequencing data for all entries, the whole amount of sequencing data following quality control is known as clean bases. The average mistake rate of a sequencing base related to quality control data is the error rate [%]. Q20 and Q30 [%] denote the sequencing quality in percentage terms of the total base, which is 99.9% and 99%, respectively; the percentage of the total bases that correspond to the quality control data for G and C bases is known as the GC content [%].

Sample	Raw reads	Clean reads	Clean bases	Error rate [%]	Q20 [%]	Q30 [%]	GC content [%]
Control_1	48 548 786	47 644 476	6 966 674 116	0.0256	97.78	93.73	44.52
Control_2	45 677 648	44 619 286	6 525 992 624	0.0255	97.80	93.81	44.50
Control_3	50 593 486	49 530 660	7 189 291 230	0.0254	97.84	93.92	44.52
CUR0_1	49 343 926	48 197 900	6 991 767 400	0.0252	97.92	94.14	44.58
CUR0_2	50 254 668	49 175 852	7 171 140 825	0.0253	97.86	93.97	44.71
CUR0_3	46 186 546	45 072 782	6 531 896 696	0.0252	97.93	94.15	44.72
CUR50_1	50 856 276	49 848 580	7 283 342 863	0.0253	97.89	94.00	44.75
CUR50_2	46 463 488	45 473 614	6 644 942 296	0.0255	97.82	93.86	44.64
CUR50_3	44 63 2956	43 646 352	6 379 182 582	0.0257	97.74	93.62	44.60

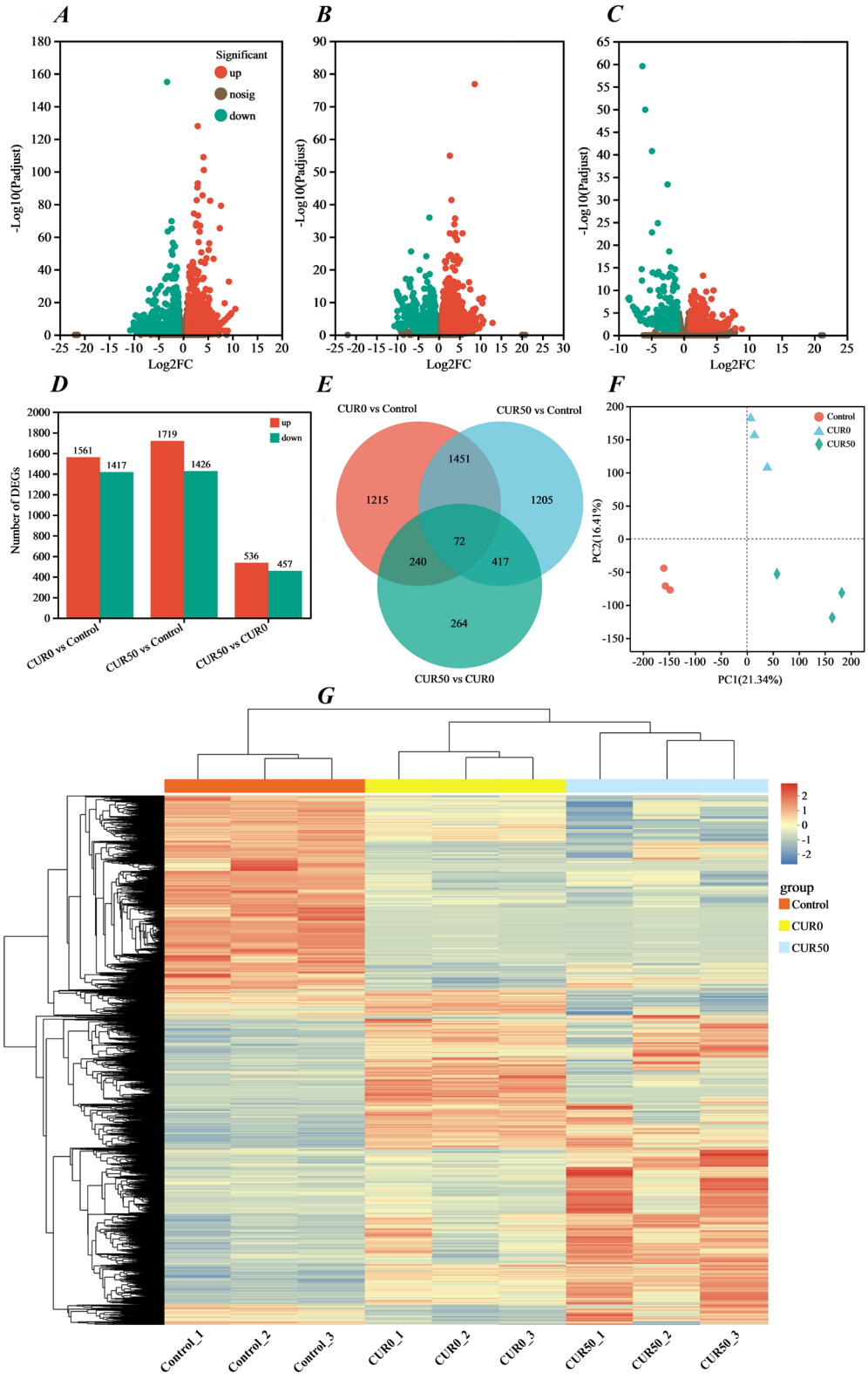

Fig. 5. Expression changes of differentially expressed genes (DEGs) in *A. trifoliata* under different treatments. Panels *A*-*C* represent volcano plots of DEGs for CUR0 *vs.* Control, CUR50 *vs.* Control, and CUR50 *vs.* CUR0 comparisons, respectively. *D*: The numbers of upregulated and downregulated DEGs. *E*: Venn diagram of the overlap of DEGs among different treatments. *F*: Principal Component Analysis (PCA). *G*: Transcriptome clustering heatmap of different replicates in the three treatments. Control group is Control; CUR0: treated with simulated acid rain having a pH of 2.0; CUR50: treated with simulated acid rain of pH 2.0 and 50 μmol/L curcumin.

shared DEGs between the CUR0 *vs.* Control and CUR50 *vs.* CUR0 comparisons (Fig. 5*E*). Additionally, 72 DEGs were shared among all three comparisons (Fig. 5*E*). The expression levels (in TPM) for Control, CUR0, and CUR50 ranged from 0 to 86 111.11, 0 to 122 433.81, and 0 to 75 044.40, respectively (Table 3 Suppl.). A distinct separation of transcriptomes between different treatments was observed in principal component analysis (PCA) and hierarchical clustering analysis, indicating significant treatment-induced alterations in the gene expression profiles of *A. trifoliata* (Fig. 5*F*,*G*).

KEGG pathway enrichment analysis of the DEGs: *KEGG* analysis was performed on the DEGs obtained from comparisons between different treatments, and a total of 115 metabolic pathways associated with these DEGs were identified. Specifically, 105 pathways were identified in the CUR0 *vs.* Control comparison, 108 pathways in the CUR50 *vs.* Control comparison, and 87 pathways in the CUR50 *vs.* CUR0 comparison. To visually represent the enrichment significance of these pathways, the top 20 pathways ranked by enrichment significance were selected for the construction of scatter plots. These pathways were classified into five major categories: genetic information processing, metabolism, environmental information processing, cellular processes, and organismal systems (Fig. 6*B*,*D*,*F*).

In the CUR0 *vs.* Control comparison, DEGs were primarily enriched in the following pathways: ribosome (map03010, 81 DEGs), phenylpropanoid biosynthesis (map00940, 25 DEGs), oxidative phosphorylation (map00190, 44 DEGs), protein processing in endoplasmic reticulum (map04141, 38 DEGs), cyanoamino acid metabolism (map00460, 11 DEGs), flavonoid biosynthesis (map00941, 7 DEGs), and plant hormone signal transduction (map04075, 32 DEGs) (Fig. 6*A*,*B*).

In the CUR50 *vs.* Control comparison, DEGs showed significant enrichment in pathways such as ribosome (86 DEGs), protein processing in endoplasmic reticulum (45 DEGs), phenylpropanoid biosynthesis (26 DEGs), oxidative phosphorylation (47 DEGs), and plant hormone signal transduction (38 DEGs) (Fig. 6*C*,*D*).

In the CUR50 *vs.* CUR0 comparison, DEGs were predominantly enriched in plant hormone signal transduction (21 DEGs), isoquinoline alkaloid biosynthesis (map00950, 8 DEGs), tyrosine metabolism (map00350, 9 DEGs), phenylpropanoid biosynthesis (11 DEGs), and cyanoamino acid metabolism (7 DEGs) (Fig. 6*E*,*F*).

We observed that a substantial number of DEGs associated with ribosome and oxidative phosphorylation pathways were downregulated in both CUR0 *vs.* Control and CUR50 *vs.* Control comparisons. These findings suggest that acid rain-induced osmotic stress and oxidative damage likely impair rRNA biosynthesis in *A. trifoliata* and reduce the efficiency of mitochondrial oxidative phosphorylation (Fig. 6*A*-*D*). In addition, both plant hormone signal transduction and phenylpropanoid biosynthesis were enriched pathways in the CUR0 *vs.* Control and CUR50 *vs.* CUR0 comparisons, and most of the DEGs involved in these two pathways were upregulated in these two comparison groups. Therefore, we speculate that the enhanced expression of genes in these two pathways may be related to the morphological and physiological changes of *A. trifoliata* under acid rain stress and the alleviating effect of CUR (Fig. 6*A*-*C*).

Key DEGs involved in plant hormone signal transduction: To elucidate the possible key regulatory factors and the molecular mechanism by which CUR alleviates acid rain stress, we analyzed the expressions of DEGs in the plant hormone signal transduction pathway in the comparisons of CUR0 *vs.* Control and CUR50 *vs.* CUR0, as shown in Fig. 7*A*. It mainly involved four plant hormone signal pathways, including auxin, cytokinin, brassinosteroid, and jasmonic acid pathways.

For the auxin signal pathway, compared with the Control group, the expression levels of one gene encoding TIR1 (TRINITY_DN694_c0_g1, members of the TIR1 family), one gene encoding IAA (TRINITY_DN51796_c0_g1, members of the Aux/IAA family), and two genes encoding GH3 (TRINITY_DN8957_c0_g1, TRINITY_DN8949_c0_g1, members of the GH3 family) were significantly upregulated under the CUR0 treatment. However, the expression levels of these genes further increased under the CUR50 treatment (Fig. 7*A*). The expression of one gene encoding ARF (TRINITY_DN53695_c0_g2, members of the ARF family) was significantly downregulated under the CUR0 treatment, but its expression level increased significantly under the CUR50 treatment. The expression levels of nine genes encoding SAUR (TRINITY_DN10506_c0_g4, TRINITY_DN7206_c0_g1, TRINITY_DN7629_c0_g2, TRINITY_DN6392_c0_g3, TRINITY_DN22869_c0_g1, TRINITY_DN6392_c0_g1, TRINITY_DN6310_c0_g1, TRINITY_DN6310_c0_g2, TRINITY_DN2368_c0_g2, members of the SAUR family) were significantly upregulated under the CUR0 treatment, but decreased under the CUR50 treatment, and the expression of TRINITY_DN7629_c0_g2 was significantly downregulated (Fig. 7*A*). In addition, compared with the CUR0 group, the expressions of three genes encoding SAUR (TRINITY_DN5178_c0_g1, TRINITY_DN20273_c0_g2, TRINITY_DN10506_c0_g3) were significantly downregulated under the CUR50 treatment, and the expression of one gene encoding GH3 (TRINITY_DN13659_c0_g1) was significantly upregulated (Fig. 7*A*).

For the cytokinin signaling pathway, compared with the Control group, the expression of two genes encoding AHK2_3_4 (members of the histidine receptor kinase family), namely TRINITY_DN42612_c1_g2 and TRINITY_DN28826_c0_g1, were significantly upregulated under the CUR0 treatment. Nevertheless, upon treatment with CUR50, these expression levels decreased, and in particular, the expression of TRINITY_DN42612_c1_g2 was notably downregulated (Fig. 7*A*). In contrast to the CUR0 group, the expression of a gene encoding AHK2_3_4, TRINITY_DN535_c0_g2, was significantly upregulated under the CUR50 treatment. Conversely, the expression levels of one gene encoding AHP (TRINITY_DN46985_c0_g2, histidine-containing

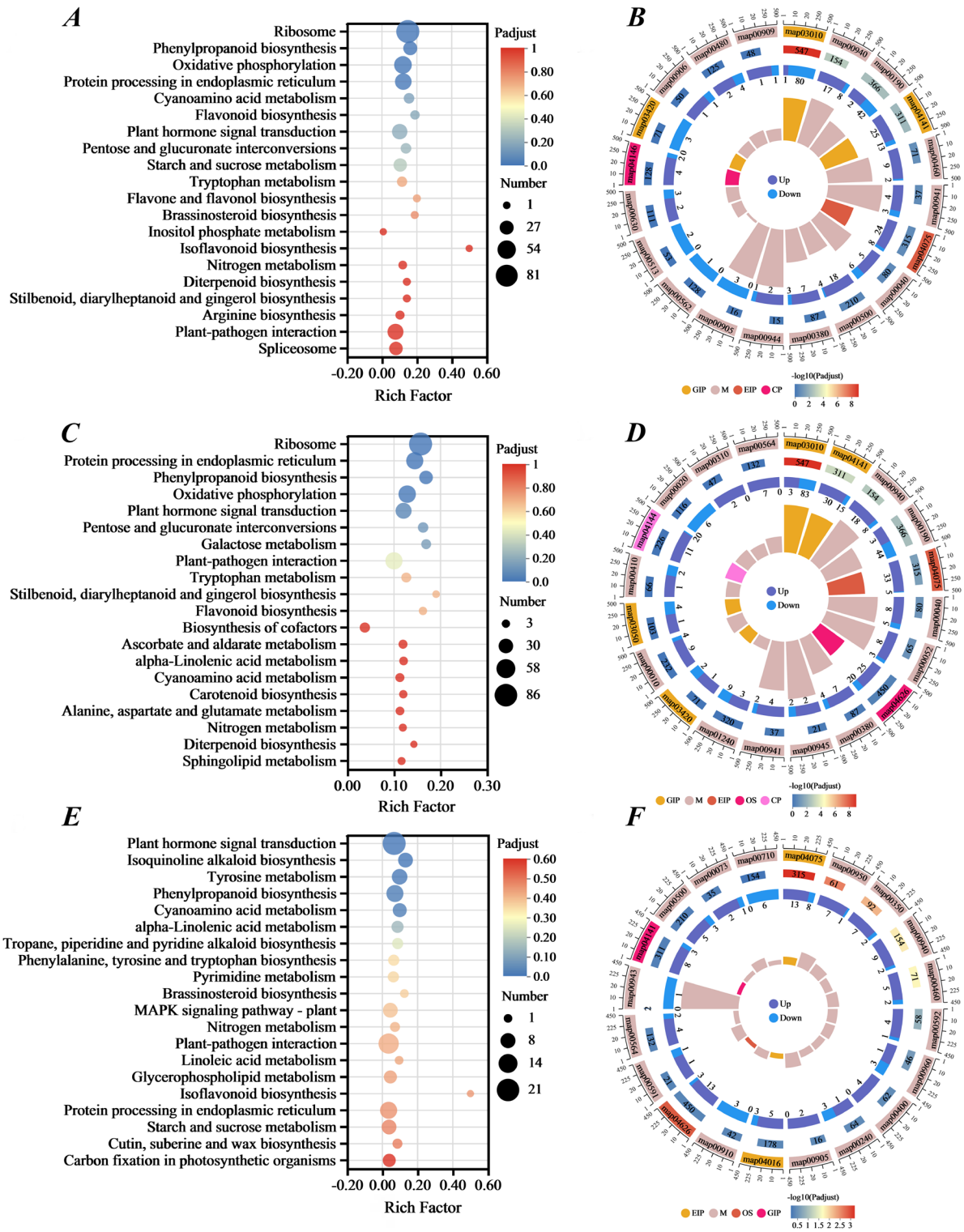

Fig. 6. *KEGG* enrichment analysis of differentially expressed genes (DEGs). *A*, *C*, and *E* represent the *KEGG* enrichment bubble plots of DEGs in the comparisons of CUR0 *vs.* Control, CUR50 *vs.* Control, and CUR50 *vs.* CUR0, respectively. *B*, *D*, and *F* represent the *KEGG* multi-dimensional enrichment circle plots of DEGs in the comparisons of CUR0 *vs.* Control, CUR50 *vs.* Control, and CUR50 *vs.* CUR0, respectively. *The first circle* represents the enriched categories. Outside the circle is the coordinate scale for the number of genes, and *different colors* represent different categories. *The second circle* indicates the number of genes in this category among the background genes and the magnitude of *Padjust*. *The third circle shows* the bar chart of the proportion of upregulated and downregulated genes. *The fourth circle* represents the Rich Factor value of each category (*i.e.*, the ratio of the number of genes enriched in this category to the number of annotated genes).

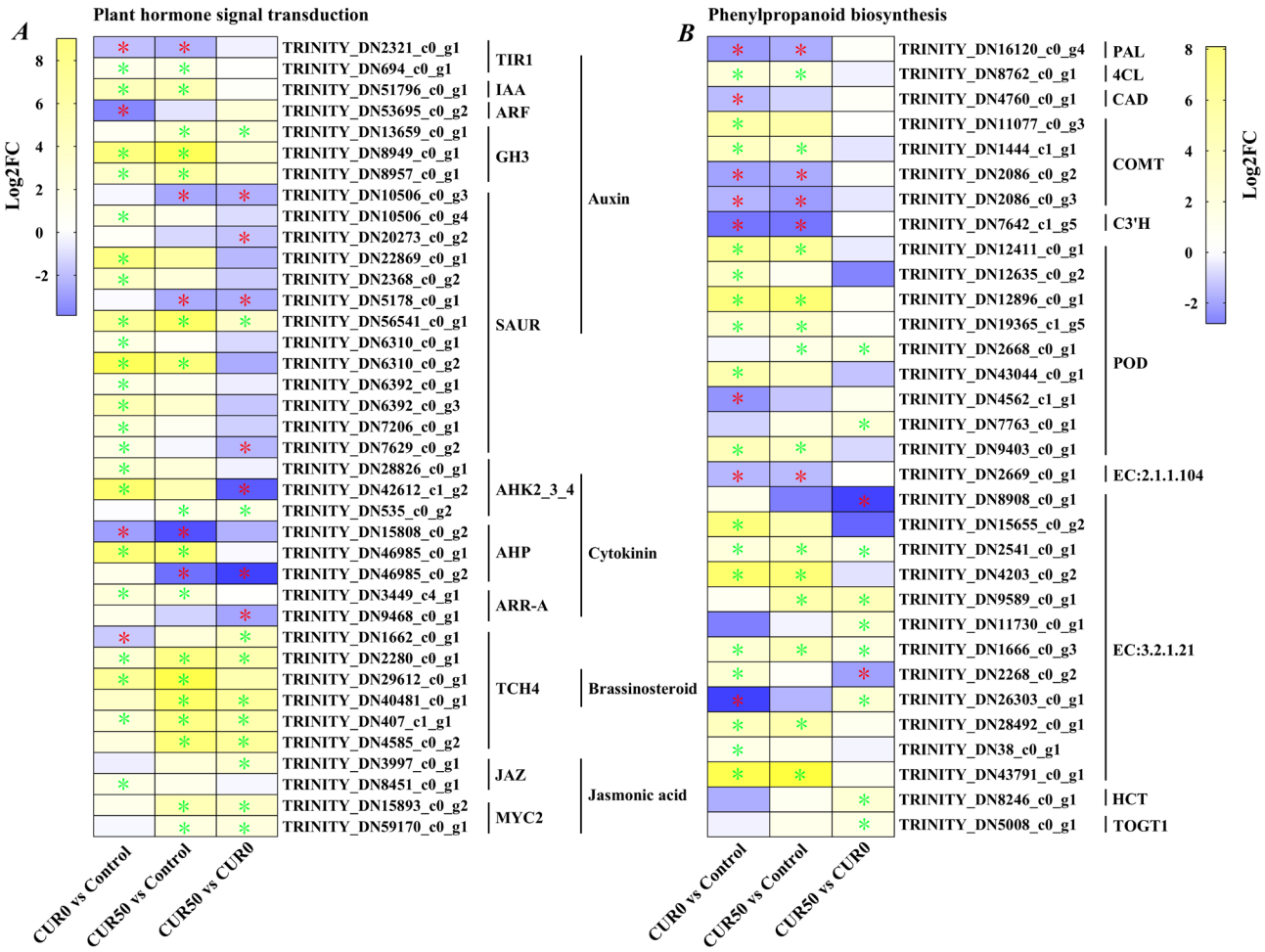

Fig. 7. Key DEGs involved in the plant hormone signal transduction and the phenylpropanoid biosynthesis pathway among different treatments. TIR1: transport inhibitor response 1 protein; IAA: auxin-responsive protein IAA; ARF: auxin response factor; GH3: auxin-responsive GH3 gene family; SAUR: SAUR family protein; AHK2_3_4: *Arabidopsis* histidine kinase 2/3/4; AHP: histidine-containing phosphotransfer protein; ARR-A: two-component response regulator ARR-A family; TCH4: xyloglucan:xyloglucosyl transferase TCH4; JAZ: jasmonate ZIM domain-containing protein; MYC2: transcription factor MYC2; PAL: phenylalanine ammonia-lyase; 4CL: 4-coumarate-CoA ligase; CAD: cinnamyl-alcohol dehydrogenase; COMT: caffeic acid 3-O-methyltransferase; C3'H: 5-O-(4-coumaroyl)-D-quinate 3'-monooxygenase; POD: peroxidase; EC 2.1.1.104: caffeoyl-CoA O-methyltransferase; EC 3.2.1.21: beta-glucosidase; HCT: shikimate O-hydroxycinnamoyltransferase; TOGT1: scopoletin glucosyltransferase. * False Discovery Rate (FDR) $P<0.05$, where *green* indicates significant upregulation and *red* indicates significant downregulation.

phosphotransfer protein) and one gene encoding ARR-A (TRINITY_DN9468_c0_g1, members of the ARR-A family) were notably downregulated (Fig. 7*A*).

For the brassinosteroid signaling pathway, genes encoding TCH4 (TRINITY_DN1662_c0_g1, TRINITY_DN2280_c0_g1, TRINITY_DN29612_c0_g1, TRINITY_DN40481_c0_g1, TRINITY_DN407_c1_g1, TRINITY_DN4585_c0_g2, members of the xyloglucan endotrans-glucosylase/hydrolase (XTH) family) exhibited low expression levels in the CUR0 group but high expression levels in the CUR50 group (Fig. 7*A*). Specifically, compared with the Control group, TRINITY_DN2280_c0_g1 and TRINITY_DN407_c1_g1 were significantly upregulated under CUR0 treatment, with their expression levels increasing by 11.84-fold and 14.51-fold, respectively, after CUR50 treatment (Fig. 7*A*). TRINITY_DN1662_c0_g1 was significantly downregulated under CUR0 treatment; however, its expression level increased 6.69-fold after CUR50 treatment (Fig. 7*A*). Additionally, the expression levels of TRINITY_DN40481_c0_g1 and TRINITY_DN4585_c0_g2 in the CUR50 group were 24.09-fold and 25.38-fold higher, respectively, than those in the CUR0 group (Fig. 7*A*).

For the jasmonic acid signaling pathway, compared with the CUR0 group, the expression levels of one gene encoding a JAZ protein (TRINITY_DN3997_c0_g1) and two genes encoding MYC2 transcription factors (TRINITY_DN59170_c0_g1, TRINITY_DN15893_c0_g2) were significantly upregulated under CUR50 treatment (Fig. 7*A*).

These results suggest that CUR may alleviate acid rain-induced damage in *A. trifoliata* by modulating the expression of plant hormone-related genes (Fig. 7*A*).

DEGs involved in phenylpropanoid biosynthesis: We further analyzed the gene expressions in the phenylpropanoid biosynthesis pathway across the CUR0 *vs.* Control and CUR50 *vs.* CUR0 comparisons, as shown in Fig. 7*B*. A total of 32 DEGs were identified, with most encoding POD (peroxidases) and EC 3.2.1.21 (beta-glucosidase). In the CUR0 group, we identified 7 POD-encoding DEGs (TRINITY_DN4562_c1_g1, TRINITY_DN12635_c0_g2, TRINITY_DN12411_c0_g1, TRINITY_DN9403_c0_g1, TRINITY_DN12896_c0_g1, TRINITY_DN43044_c0_g1, TRINITY_DN19365_c1_g5) and 9 EC 3.2.1.21-encoding DEGs (TRINITY_DN26303_c0_g1, TRINITY_DN4203_c0_g2, TRINITY_DN15655_c0_g2, TRINITY_DN2541_c0_g1, TRINITY_DN43791_c0_g1, TRINITY_DN2268_c0_g2, TRINITY_DN38_c0_g1, TRINITY_DN28492_c0_g1, TRINITY_DN1666_c0_g3). Among these, all genes were upregulated except TRINITY_DN4562_c1_g1 and TRINITY_DN26303_c0_g1, which were downregulated (Fig. 7*B*). In the CUR50 treatment group (compared to CUR0), we identified 2 POD-encoding DEGs (TRINITY_DN7763_c0_g1, TRINITY_DN2668_c0_g1) and 7 EC 3.2.1.21-encoding DEGs (TRINITY_DN9589_c0_g1, TRINITY_DN2541_c0_g1, TRINITY_DN11730_c0_g1, TRINITY_DN26303_c0_g1, TRINITY_DN1666_c0_g3, TRINITY_DN8908_c0_g1, TRINITY_DN2268_c0_g2). All genes were upregulated except TRINITY_DN8908_c0_g1 and TRINITY_DN2268_c0_g2, which were downregulated (Fig. 7*B*).

These results indicate that *A. trifoliata* may enhance acid rain tolerance by regulating lignin- and coumarin-related gene expression under stress. Furthermore, CUR treatment modulates the expression of these genes, thereby alleviating acid rain-induced damage.

Discussion

Acid rain stress inhibits plant growth by inducing osmotic stress and oxidative damage. The most direct effect of acid rain stress on plants is on leaves, causing serious damage to the integrity of anatomical structure of leaves (Ren et al., 2021). In this study, *A. trifoliata* plant growth and development were significantly inhibited under acid rain stress, resulting in decreased biomass and a large number of white-brown necrotic spots on the leaves. The addition of exogenous CUR significantly decreased the damage to *A. trifoliata* leaves. Both CUR25 and CUR50 could significantly reduce necrotic spots on the leaves and increase the biomass, whereas the necrotic spots were significantly higher in CUR100 than in CUR25 and CUR50. Additionally, the root system of *A. trifoliata* was severely distorted in CUR100. This might be because the high concentration of CUR caused oxidative damage to the root system of *A. trifoliata*, leading to the destruction of the structure of newly formed cells (such as root primordium cells). This suggested that the appropriate concentration of CUR could effectively alleviate the damage due to acid rain stress on *A. trifoliata*; however, the effect was weakened when CUR concentration was too high. This was consistent with the results obtained by Zhang et al. (2024) in spinach.

Chlorophyll is an important pigment for photosynthesis in plants. Its content is an important basis for assessing growth, development, and physiological condition of plants (Gharibiyan et al., 2023). In this study, acid rain stress alone significantly reduced the chlorophyll content of *A. trifoliata* leaves. This could be because of two reasons. First, acid rain directly damages photosynthetic apparatus through chemical erosion, resulting in impaired photosynthetic efficiency. Second, the chloroplast was damaged when the plant was under stress, and the activity of chlorophyll-degrading enzyme increased, which accelerated chlorophyll degradation (dos Santos et al., 2023). In this study, the content of chlorophyll *a*, chlorophyll *b*, and total chlorophyll in *A. trifoliata* leaves significantly increased under acid rain stress after CUR25 and CUR50 treatments. However, the chlorophyll content significantly reduced in CUR100, which was consistent with the degree of spot necrosis of plant leaves and changes in root morphology. The effect of increasing chlorophyll content was the best in CUR50, demonstrating that the appropriate concentration of CUR could effectively reduce the inhibitory effect of acid rain stress on the growth of *A. trifoliata*.

Osmoregulation plays an important role in the stress resistance of plants mainly *via* two aspects. First, it improves plants' water absorption capacity through osmotic pressure regulation. Second, it maintains the integrity of cell structure and function through osmotic protection (Lambers et al., 2006). Soluble sugar and soluble protein are important intracellular osmoregulatory substances, and increase in their content is favorable for the tolerance of plants to acid rain stress (Du et al., 2023). Accumulation of proline, which is very sensitive to changes in the external environment, reflects the adversity resistance of plants (Maach et al., 2020). In this study, acid rain stress alone accelerated starch degradation and significantly increased the content of soluble sugar, soluble protein, and proline in *A. trifoliata* leaves. This was conducive to cope with acid rain stress. The application of exogenous CUR further increased the content of soluble sugar, soluble protein, and proline. Particularly, CUR50 exhibited the highest content of these substances. This indicated that CUR could promote the biosynthesis of osmoregulatory substances under acid rain stress, thereby maintaining the osmotic balance and integrity of cell structure and function.

Under normal conditions, the ROS content in plants is relatively low, which plays an important role in maintaining the intracellular physiological balance. Under acid rain stress, plants produce more ROS, exacerbating the degree of membrane lipid peroxidation, leading to cell death, and thus inhibiting plant growth (Debnath et al., 2018). Oxygen free radicals and MDA are important indicators of membrane lipid peroxidation levels and degree of damage (Wang et al., 2023). In this study, the MDA content and production rate of oxygen free radicals were significantly higher in CUR0 than in Control. This suggested that acid rain stress led to more ROS production in *A. trifoliata* leaves, disrupted the physiological balance, and increased

cell membrane permeability. CUR25 and CUR50 effectively reduced the MDA content and production rate of oxygen free radicals in *A. trifoliata* leaves, with CUR50 being the most effective. This may be related to the direct scavenging of free radicals by CUR (Zaki et al., 2023). Overall, exogenous CUR played important roles in reducing ROS, minimizing plasma membrane damage, and protecting and repairing cell membranes.

SOD, POD, and CAT are important components of the antioxidant defense system and play a role in protecting the stability and integrity of cell membranes under stress conditions (Zhang et al., 2017). In this study, under acid rain stress alone, the activities of SOD, POD, and CAT were elevated in *A. trifoliata* leaves. This suggested that injury to *A. trifoliata* leaves and stress response simultaneously occurred, increasing the activity of antioxidant enzymes and weakening the harmful effects of acid rain stress. Exogenous CUR could further effectively increase the activities of SOD, POD, and CAT, thus effectively reducing the damage caused by acid rain stress to *A. trifoliata* and playing a protective role. However, the effect was dependent on the concentration of CUR. The activities of the three antioxidant enzymes were the highest in CUR50. In summary, the comprehensive evaluation of changes in plant morphology, content of chlorophyll, osmoregulatory substances, and membrane lipid peroxidation products, activity of antioxidant enzymes, and physiological indexes indicated that CUR50 was an optimal treatment exhibiting important mitigation effect on the damage due to acid rain stress in *A. trifoliata*.

In the process of plant growth and development, the leaf is one of the most sensitive organs to environmental changes. Observing leaf anatomical structures and analyzing interrelationships between tissues constitute one of the most intuitive approaches to investigate the extent of plant damage under stress conditions (Li et al., 2022). In this study, the leaves of *A. trifoliata* (Control) grown under normal conditions were relatively thin, and the leaf epidermis was completely wrapped around the periphery of the entire leaf blade and played a protective role. The palisade tissues consisted of 1-2 layers of long columnar or ellipsoidal cells, which were mainly involved in photosynthesis. However, under acid rain stress alone, the epidermis and lateral veins of *A. trifoliata* leaves were severely damaged, and the leaf thickness significantly increased. The palisade tissues mostly consisted of two layers of long columnar cells, which were more compact, and the ratio of palisade/spongy tissues significantly increased. Indeed, thickening of leaves, increase in the number of palisade tissues, and shortening of intercellular spaces could help to improve the plant's water utilization rate. Meanwhile, the increase in leaf thickness also helps reduce excessive water transpiration (Dong and Zhang, 2001). Thus, acid rain stress may cause severe physiological water deficit in *A. trifoliata*; however, *A. trifoliata* may reduce water consumption by increasing leaf thickness and water transport efficiency by thickening palisade tissues and shortening intercellular spaces. In CUR50, the structural integrity of leaves under acid rain stress remained basically intact, whereas the growth of palisade tissues in terms of thickness gradually slowed down. This indicated that exogenous CUR could alleviate the damage due to acid rain stress to the tissue structure of *A. trifoliata* leaves.

Under abiotic stress, plants regulate the expression of relevant genes to regulate the physiological and biochemical mechanisms involving various metabolism pathways to alleviate the damage caused by external environmental changes. Ribosomes play an important role in plant metabolism by translating mRNA into functional proteins (Ramakrishnan, 2002). Additionally, external stress may lead to increased activity of uncoupling proteins in plant mitochondria and uncoupling of oxidative phosphorylation. This results in decreased oxidative phosphorylation efficiency of mitochondria, thereby affecting the normal energy metabolism of cells (Jacoby et al., 2011). In this study, most of the differentially expressed genes (DEGs) involved in the ribosome and oxidative phosphorylation pathways were downregulated in CUR0 *vs*. Control and CUR50 *vs*. Control, with multiple relevant DEGs. Hence, it was deduced that osmotic stress and oxidative damage induced by acid rain stress may mainly impair the rRNA biosynthesis and reduce the oxidative phosphorylation efficiency of mitochondria in *A. trifoliata*.

Numerous studies have demonstrated that phytohormones play pivotal roles in modulating stress responses and activating downstream signaling pathways. Key regulators such as auxin, cytokinins, brassinosteroids, and jasmonates critically integrate plant developmental processes with physiological adaptations under stress conditions (Hajam et al., 2024; Sim et al., 2024; Tan et al., 2024). As an important signaling molecule in plants, auxin not only orchestrates growth and developmental processes but also plays a significant role in regulatory mechanisms enabling plants to adapt to environmental stress (Ren and Gray, 2015). Early auxin-responsive genes, such as GH3, AUX/IAA, and SAUR, play crucial regulatory roles in the auxin signaling pathway (Chapman and Estelle, 2009). Under stress conditions, AUX/IAA, as a transcriptional repressor, regulates the expression of auxin-responsive genes by inhibiting the activity of ARF transcription factors (Mano and Nemoto, 2012). GH3 proteins regulate auxin homeostasis through a negative feedback mechanism and are involved in plant stress responses (Tan et al., 2024). SAUR represents the largest gene family among early auxin-responsive factors, with certain members, such as SAUR39 in rice, acting as negative regulators of auxin biosynthesis and transport (Kant et al., 2009). This study analyzed the expression levels of genes encoding IAA, ARF, GH3, and SAUR in the auxin signaling pathway. Compared to the Control group, the CUR0 treatment group exhibited upregulation of DEGs encoding IAA, GH3, and SAUR, while DEGs encoding ARF were downregulated. Additionally, based on plant growth phenotypic data, biomass was significantly reduced under CUR0 treatment. These results suggest that acid rain stress may inhibit auxin signal transduction, thereby restricting the growth of *A. trifoliata*. In contrast, compared to the CUR0 group, the expression levels of most SAUR-encoding genes

were markedly reduced in the CUR50 treatment group, and plant biomass significantly increased. This indicates that CUR may alleviate acid rain stress by mitigating its inhibitory effects on auxin signal transduction, thereby exerting a protective effect.

Brassinosteroids are a class of polyhydroxylated sterol phytohormones that play a critical role in enhancing plant abiotic stress tolerance (Iliev et al., 2002; Divi and Krishna, 2009). TCH4, a downstream responsive factor in the brassinosteroid signaling pathway, exhibits elevated expression levels regulated by brassinosteroids, auxin, and stress conditions (Xu et al., 1995). In response to environmental stress, TCH4 may modify the cell wall (*e.g.*, by regulating the structure and cross-linking of xyloglucans), thereby enhancing its mechanical strength and elasticity, which helps plants adapt to stress conditions (Iliev et al., 2002). In this study, compared to the Control group, most DEGs encoding TCH4 were upregulated under CUR0 treatment. These results suggest that TCH4 genes may be highly sensitive to acid rain stress. Compared to the CUR0 group, all DEGs encoding TCH4 in the CUR50 treatment group exhibited upregulated expression with significantly increased levels, accompanied by a substantial reduction in leaf damage and relatively intact leaf anatomical structures. Therefore, we speculate that CUR may function similarly to brassinosteroids and auxin in alleviating plant stress, although its specific mechanisms require further validation.

In plants, almost all types of defensive secondary metabolites need to be synthesized either directly or indirectly *via* the phenylpropanoid metabolic pathway (Yadav et al., 2020). POD is a key enzyme in the synthesis of lignin within the phenylpropanoid metabolic pathway, and it can catalyze the polymerization of lignin monomers into high-molecular-weight lignin (Xin et al., 2022). Lignin, on the other hand, widely mediates the responses of plants to abiotic stresses (Dong et al., 2023). During the process of lignin synthesis, the relevant phenylpropanoid precursor substances mostly exist in the form of glycoside conjugates. EC 3.2.1.21 may hydrolyze these glycoside conjugates, releasing the lignin precursors, thereby promoting the synthesis of lignin (Escamilla-Treviño et al., 2006). In this study, most genes in the phenylpropanoid pathway encoded POD and EC 3.2.1.21. Compared with the Control group, most of the DEGs encoding POD and EC 3.2.1.21 were upregulated under CUR0 treatment. This result indicates that the enhanced expression of these genes may be beneficial for lignin synthesis, thus reducing the damage caused by stress. In comparison to the CUR0 group, many highly expressed genes of POD and EC 3.2.1.21 were also identified in the CUR50 treatment group. In conclusion, CUR has potential effects in multiple aspects of alleviating acid rain stress in *A. trifoliata*.

Conclusions

Physiological, anatomical, and transcriptomic analyses revealed that acid rain stress significantly inhibited the normal growth of *A. trifoliata*. It led to chlorosis, large numbers of white-brown spots, chlorophyll degradation, and excessive accumulation of membrane lipid peroxidation products in the leaves. It destroyed the structural integrity of the upper and lower epidermis and lateral veins of the leaves and significantly downregulated the DEGs involved in ribosome and oxidative phosphorylation metabolism. Further, the tolerance mechanism of *A. trifoliata* to acid rain stress was investigated. Under acid rain stress, content of osmoregulatory substances and activities of antioxidant enzymes increased, the leaf blade was significantly thickened, the number of palisade tissue layers significantly increased, the cell morphology was altered, the intercellular spaces became smaller, and the ratio of palisade/spongy tissues increased. Transcriptomic analysis revealed that various DEGs related to abiotic stress, including those from plant hormone signal transduction and phenylpropanoid biosynthesis pathways, were upregulated. The DEGs encoding IAA, ARF, GH3, SAUR, TCH4, and POD were important factors involved in this mechanism. Meanwhile, appropriate concentration of exogenous CUR could effectively improve plant growth, slow down the degradation rate of chlorophyll, and increase the contents of osmoregulatory substances and antioxidant enzyme activity. Thus, it maintained the osmotic balance and integrity of the anatomical structure of the leaves, lowered the degree of cell membrane lipid peroxidation, and alleviated the damage due to acid rain stress in *A. trifoliata*. The most significant effect was observed at 50 μmol/L of CUR. Additionally, genes involved in protein processing in endoplasmic reticulum, plant hormone signal transduction, phenylpropanoid biosynthesis, and starch and sucrose metabolism pathways were regulated by exogenous CUR, indicating that exogenous CUR could mitigate the effects of acid rain stress in *A. trifoliata via* these pathways.

References

Anas, M., Falak, A., Khan, A. et al. (2024) Therapeutic potential and agricultural benefits of curcumin: a comprehensive review of health and sustainability applications. *Journal of Umm Al-Qura University for Applied Sciences*.

Cai, F., Zou, S., Gao, P. et al. (2022) [Analysis on quality variations of *Akebia trifoliata* fruit at different harvesting times.] *Journal of Plant Resources and Environment*, 31, 83-85. [In Chinese]

Chapman, E.J. & Estelle, M. (2009) Mechanism of auxin-regulated gene expression in plants. *Annual Review of Genetics*, 43, 265-285.

Debnath, B., Hussain, M., Irshad, M. et al. (2018) Exogenous melatonin mitigates acid rain stress to tomato plants through modulation of leaf ultrastructure, photosynthesis and antioxidant potential. *Molecules*, 23, 388.

Divi, U.K. & Krishna, P. (2009) Brassinosteroid: a biotechnological target for enhancing crop yield and stress tolerance. *New Biotechnology*, 26, 131-136.

Dong, Q., Wu, Y., Li, B. et al. (2023) Multiple insights into lignin-mediated cadmium detoxification in rice (*Oryza sativa*). *Journal of Hazardous Materials*, 458, 131931.

Dong, X. & Zhang, X. (2001) Some observations of the adaptations of sandy shrubs to the arid environment in

the Mu Us Sandland: Leaf water relations and anatomic features. *Journal of Arid Environments*, 48, 41-48.
dos Santos, L.A., Batista, B.L. & Lobato, A.K.D.S. (2023) 24-Epibrasinolide delays chlorophyll degradation and stimulates the photosynthetic machinery in magnesium-stressed soybean plants. *Journal of Plant Growth Regulation*, 42, 183-198.
Du, X., Chen, H., Qin, X., Xu, W. & Luo, Q. (2023) [Physiological and biochemical response of *Enteromorpha* and *Ulva* to simulated acid rain stress.] *Journal of Nuclear Agricultural Sciences*, 37, 1067-1075. [In Chinese]
Du, Y., Zhao, Q., Chen, L. et al. (2020) Effect of drought stress on sugar metabolism in leaves and roots of soybean seedlings. *Plant Physiology and Biochemistry*, 146, 1-12.
Escamilla-Treviño, L.L., Chen, W., Card, M.L., Shih, M.C. & Poulton, J.E. (2006) *Arabidopsis thaliana* β-glucosidases BGLU45 and BGLU46 hydrolyse monolignol glucosides. *Phytochemistry*, 67, 1651-1660.
Gao, J. (2006) [Plant Physiology Experiment Guidance.] Beijing: Higher Education Press, pp. 140-148. [In Chinese]
Gharibiyan, P., Roozban, M.R., Rahemi, M. & Vahdati, K. (2023) Exogenous salicylic acid improves growth and physiological status of two *Pistacia* species under salinity stress. *Erwerbs-Obstbau*, 65, 1441-1452.
Hajam, A.H., Ali, M.S., Singh, S.K. & Bashri, G. (2024) Understanding cytokinin: Biosynthesis, signal transduction, growth regulation, and phytohormonal crosstalk under heavy metal stress. *Environmental and Experimental Botany*, 228, 106025.
Hu, Y., Yang, L., Gao, C. et al. (2022) A comparative study on the leaf anatomical structure of *Camellia oleifera* in a low-hot valley area in Guizhou Province, China. *PLoS ONE*, 17, e0262509.
Iliev, E.A., Xu, W., Polisensky, D.H. et al. (2002) Transcriptional and posttranscriptional regulation of *Arabidopsis TCH4* expression by diverse stimuli. Roles of cis regions and brassinosteroids. *Plant Physiology*, 130, 770-783.
Jacoby, R.P., Taylor, N.L. & Millar, A.H. (2011) The role of mitochondrial respiration in salinity tolerance. *Trends in Plant Science*, 16, 614-623.
Jia, Y., Yang, Q., Zeng, L. et al. (2022) [Triterpenes from stems of *Akebia trifoliata* and their antibacterial activities.] *Journal of Tropical and Subtropical Botany*, 30, 144-150. [In Chinese]
Kant, S., Bi, Y.-M., Zhu, T. & Rothstein, S.J. (2009) *SAUR39*, a small auxin-up RNA gene, acts as a negative regulator of auxin synthesis and transport in rice. *Plant Physiology*, 151, 691-701.
Kováčik, J., Klejdus, B., Bačkor, M., Štork, F. & Hedbavny, J. (2011) Physiological responses of root-less epiphytic plants to acid rain. *Ecotoxicology*, 20, 348-357.
Kumar, G.N.M. & Knowles, N.R. (1993) Changes in lipid peroxidation and lipolytic and free-radical scavenging enzyme activities during aging and sprouting of potato (*Solanum tuberosum*) seed-tubers. *Plant Physiology*, 102, 115-124.
Lambers, H., Shane, M.W., Cramer, M.D., Pearse, S.J. & Veneklaas, E.J. (2006) Root structure and functioning for efficient acquisition of phosphorus: Matching morphological and physiological traits. *Annals of Botany*, 98, 693-713.
Langmead, B. & Salzberg, S.L. (2012) Fast gapped-read alignment with Bowtie 2. *Nature Methods*, 9, 357-359.
Li, B. & Dewey, C.N. (2011) RSEM: accurate transcript quantification from RNA-Seq data with or without a reference genome. *BMC Bioinformatics*, 12, 323.
Li, H. (2000) [Principles and Techniques of Plant Physiology and Biochemistry Experiments.] Beijing: Higher Education Press, pp. 164-165. [In Chinese]
Li, R., Wang, Y., Sun, Y., Zhang, L. & Chen, A. (2022) [Effects of salt stress on leaf morphology and anatomical structure of *Bromus inermis* seedlings.] *Acta Agrestia Sinica*, 30, 1450-1459. [In Chinese]
Maach, M., Baghour, M., Akodad, M. et al. (2020) Overexpression of *LeNHX4* improved yield, fruit quality and salt tolerance in tomato plants (*Solanum lycopersicum* L.). *Molecular Biology Reports*, 47, 4145-4153.
Mano, Y. & Nemoto, K. (2012) The pathway of auxin biosynthesis in plants. *Journal of Experimental Botany*, 63, 2853-2872.
Polishchuk, O.V., Vodka, M.V., Belyavskaya, N.A., Khomochkin, A.P. & Zolotareva, E.K. (2016) The effect of acid rain on ultrastructure and functional parameters of photosynthetic apparatus in pea leaves. *Cell and Tissue Biology*, 10, 250-257.
Qian, C., Zhao, L., Yang, Y., Han, B., Wu, J. & Ou, J. (2022) [Analysis of the transcriptome and discovery of key enzyme genes of the triterpenoid saponin biosynthesis pathway in *Akebia trifoliata* (Thunb.) Koidz.] *Plant Science Journal*, 40, 378-389. [In Chinese]
Ramakrishnan, V. (2002) Ribosome structure and the mechanism of translation. *Cell*, 108, 557-572.
Ren, H. & Gray, W.M. (2015) SAUR proteins as effectors of hormonal and environmental signals in plant growth. *Molecular Plant*, 8, 1153-1164.
Ren, X., Zhang, J., Xiang, H., Shi, Z., Hei, Z. & Li, M. (2021) [Research advances and prospects for effects of acid rain on aboveground physiology of plants and related alleviation countermeasures.] *Chinese Journal of Applied and Environmental Biology*, 27, 1716-1724. [In Chinese]
Sim, Y., Min, K. & Lee, E.J. (2024) Salicylic acid and transcriptional activation of phytohormone signalling potentially mediate chilling response in cucumber fruit peel. *Postharvest Biology and Technology*, 218, 113182.
Tan, X., Long, W., Ma, N., Sang, S. & Cai, S. (2024) Transcriptome analysis suggested that lncRNAs regulate rapeseed seedlings in responding to drought stress by coordinating the phytohormone signal transduction pathways. *BMC Genomics*, 25, 704.
Wang, D., Zhang, W., Zhang, R., Tao, N., Si, L. & Guo, C. (2023) Phytotoxicity of nitrobenzene bioaccumulation in rice seedlings: Nitrobenzene inhibits growth, induces oxidative stress, and reduces photosynthetic pigment synthesis. *Plant Physiology and Biochemistry*, 204, 108096.
Wang, L. (2024) [Physiological Characteristics and Seedling-Stage Transcriptomic Analysis of *Cyperus esculentus* under Alkali Stress throughout the Growth Period.] Changchun: Jilin Agricultural University, pp. 67. [In Chinese]
Wu, Z., Yu, L., Yan, L., Zhou, C., Cai, G. & Zhang, J. (2018) [Responses of *Akebia trifoliata* leaf anatomical structure and photosynthetic characteristic to drought stress.] *Journal of Southern Agriculture*, 49, 1156-1163. [In Chinese]
Xiao, S., Wang, G.G., Tang, C., Fang, H., Duan, J. & Yu, X. (2020) Effects of one-year simulated nitrogen and acid deposition on soil respiration in a subtropical plantation in China. Forests, 11, 235.
Xin, J., Li, Y., Zhao, C. & Tian, R. (2022) [Transcriptome sequencing in the leaves of *Pontederia cordata* with cadmium exposure and gene mining in phenylpropanoid pathways.] *Biotechnology Bulletin*, 38, 198-210. [In Chinese]
Xu, W., Purugganan, M.M., Polisensky, D.H., Antosiewicz, D.M., Fry, S.C. & Braam, J. (1995) *Arabidopsis TCH4*, regulated by hormones and the environment, encodes a xyloglucan endotransglycosylase. *The Plant Cell*, 7, 1555-1567.
Yadav, V., Wang, Z., Wei, C. et al. (2020) Phenylpropanoid pathway engineering: an emerging approach towards plant defense. *Pathogens*, 9, 312.

Yao, L., Wang, X., Zhuo, C., Leng, M. & Ni, W. (2022) [Effects of simulated acid rain on dissolution characteristics and fraction of phosphorus in tea garden soil.] *Acta Agriculturae Zhejiangensis*, 34, 2700-2709. [In Chinese]

Zaki, F.S., Khater, M.A., EI-Awadi, M.E., Dawood, M.G. & Elsayed, A.E. (2023) Curcumin-polyvinyl alcohol nano-composite enhances tolerance of *Helianthus annuus* L. against salinity stress. *Beni-Suef University Journal of Basic and Applied Sciences*, 12, 60.

Zhang, L., Zengin, G., Ozfidan-Konakci, C. et al. (2024) Exogenous curcumin mitigates As stress in spinach plants: A biochemical and metabolomics investigation. *Plant Physiology and Biochemistry*, 211, 108713.

Zhang, Y. (2024) [Creation of autotetraploid *Akebia trifoliata* and analysis of differentially expressed genes.] Ya'an: Sichuan Agricultural University, pp. 64. [In Chinese]

Zhang, Y.P., Yang, S.J. & Chen, Y.Y. (2017) Effects of melatonin on photosynthetic performance and antioxidants in melon during cold and recovery. *Biologia Plantarum*, 61, 571-578.

Zhang, Z., Chai, X., Zhang, B. et al. (2023) Potential role of root-associated bacterial communities in adjustments of desert plant physiology to osmotic stress. *Plant Physiology and Biochemistry*, 204, 108124.

Zhang, Z., Qu, W & Li, X. (2009) [Plant Physiology Experiment Guidance.] 4th Edition. Beijing: Higher Education Press, pp. 223-224. [In Chinese]

Zhou, X., Xu, Z., Liu, W., Wu, Y., Zhao, T. & Jiang, H. (2017) [Progress in the studies of precipitation chemistry in acid rain areas of southwest China.] *Environmental Science*, 38, 4438-4446. [In Chinese]

Zou, Q. (2000) [Plant Physiology Experiment Guidance.] Beijing: China Agriculture Press, pp. 72-170. [In Chinese]